IEEE Access
Multidisciplinary ⋮ Rapid Review ⋮ Open Access Journal

Received 5 June 2024, accepted 18 June 2024, date of publication 26 June 2024, date of current version 26 July 2024.

Digital Object Identifier 10.1109/ACCESS.2024.3419444

RESEARCH ARTICLE

Combining Proportional-Integral, Deadbeat, and Repetitive Current Controllers in Energy-Storage-Equipped STATCOM Application

HIKMAT BASNET, (Graduate Student Member, IEEE), AND TOMI ROINILA, (Member, IEEE)
Department of Electrical Engineering, Tampere University, 33014 Tampere, Finland
Corresponding author: Hikmat Basnet (hikmat.basnet@tuni.fi)

ABSTRACT Energy-storage-equipped static synchronous compensators (E-STATCOM) are crucial devices in a modern power grid for regulating both the active and reactive power, thereby improving the efficiency and power quality. Current controllers commonly used with E-STATCOM devices include proportional-integral (PI), repetitive, and deadbeat controllers. However, each has application-dependent restrictions and therefore lack the ability to achieve optimal operation. This paper presents a novel hybrid current controller that combines the strengths of the PI, deadbeat, and repetitive controllers. The proposed current controller mitigates cross-coupling effects and provides a wide control bandwidth, thereby ensuring quick, precise, and robust response to system parameter variations. Moreover, the proposed controller provides an efficient disturbance rejection, presenting a holistic solution for enhanced performance of the E-STATCOM. The proposed controller not only overcomes the limitations of individual controllers, but also provides improved current regulation. A comparative analysis of the proposed hybrid controller and a conventional repetitive controller clearly shows the efficiency of the proposed technique. Experimental findings based on a three-phase E-STATCOM demonstrate that the proposed controller significantly minimizes cross-coupling effects and provides approximately 150 % higher bandwidth compared to the conventional controller. In addition, applying the proposed controller shows 3 % and 6 % of total harmonic distortions (THD) during normal system operation and during periodic disturbances, respectively, which is approximately 38 % lower than the THD observed with the conventional controller.

INDEX TERMS STATCOM, energy storage, current control, dSpace, Imperix Boombox.

NOMENCLATURE

DAB	Dual Active Bridge.
DB-PI	Proportional-Integral Based Deadbeat.
DFT	Discrete Fourier Transform.
ESS	Energy Storage System.
PCC	Point of Common Coupling.
PHIL	Power Hardware-In-The-Loop.
PI	Proportional-Integral.
PLL	Phase-Locked Loop.
PWM	Pulse-Width Modulation.
RC	Repetitive Controller.
RCFF	Reference Current Feed-Forward.
STATCOM	Static Synchronous Compensator.
THD	Total Harmonic Distortion.
VSC	Voltage Source Converter.

The associate editor coordinating the review of this manuscript and approving it for publication was Behnam Mohammadi-Ivatloo.

I. INTRODUCTION

Energy-storage-equipped static synchronous compensators (E-STATCOMs) are often employed in modern high-voltage transmission systems, where they can mitigate voltage stability issues and improve the system performance by regulating active and reactive power [1]. E-STATCOMs are

essential devices for enhancing the reliability and efficiency of various power systems, especially in the presence of renewable energy sources and other dynamic loads.

In its simplest form, an E-STATCOM device consists of a voltage source converter (VSC), a DC-link capacitor, and an energy-storage system (ESS) on the DC side [2]. Unlike conventional STATCOMs, the E-STATCOM can store additional energy when the demand is low and release stored energy when demand increases or during voltage fluctuations. This dual functionality deals with the unpredictable nature of renewable energy sources, smoothing out fluctuations, and ensuring a stable power supply to the grid [3]. The ability to store and discharge energy rapidly enhances the overall responsiveness and flexibility of the STATCOM.

Two of the most popular current controllers used in STATCOM applications are the proportional-integral (PI) controller and the deadbeat controller [4]. The PI controller is simple and effective [5], whereas the deadbeat controller offers fast dynamic response and low current harmonics [6]. However, the PI controller usually has a smaller bandwidth, making it vulnerable to variations in the system [7]. On the other hand, the deadbeat controller suffers from a delay that affects the controller performance [8]. Moreover, both the PI and deadbeat controllers do not perform well in the presence of periodic disturbances such as harmonics and fluctuations in grid voltage.

An effective technique to mitigate the impact of periodic disturbances is to apply a repetitive controller (RC) [9], [10]. The RC is one type of linear controller that is based on the internal model principle [11]. The internal model typically takes the form of a filter or transfer function that closely matches the frequency and phase characteristics of the repetitive disturbance. By introducing this internal model into the controller, the system can more efficiently predict and cancel out the effects of the periodic disturbances [12]. Moreover, a well-designed single RC can eliminate a wide range of harmonics compared to a bank of resonant controllers used for the same purpose [13], [14].

Recent advancements in RCs have significantly enhanced their application in inverter-based systems to mitigate harmonic distortion. The integration of a frequency-adaptive RC with a dead-beat controller, as demonstrated in [15], enables rapid and precise control of inverters in the vehicle-to-grid applications. Similarly, RCs combined with PI controllers, such as in [16], have effectively addressed sub-synchronous oscillations in wind power systems. A notable innovation is the discrete-time RC proposed in [16]. When paired with the extended state observer, it effectively suppresses both AC and DC disturbances in permanent magnet motor applications.

Further advancements include the virtual even-order fractional RC integrated with a PI controller, as introduced in [18]. This configuration replaces the conventional low-pass filter with a finite-impulse response filter, thereby enhancing convergence rates and the efficiency of harmonic suppression. In [19], the development of a model predictive repetitive controller has been shown to bolster system robustness and energy quality. Likewise, integrating an RC with predictive current control, as seen in [20], has enhanced the performance of grid-connected inverters under distorted voltage conditions.

Moreover, the adaptive plug-in RC presented in [21] offers a sophisticated solution to the challenge of frequency fluctuations, showcasing the versatility and adaptability of RCs in various applications. Despite these substantial advancements, the implementation of RCs is still constrained by their inherent narrow bandwidth and significant delays, which have an adverse effect on the system's dynamic performance. Consequently, ongoing research is crucial to address these limitations and further enhance the efficacy of RC-integrated controllers.

This paper presents a novel control solution for an E-STATCOM by combining the PI, deadbeat, and repetitive current controllers. The proposed hybrid current controller employs the decoupling mechanism of PI control, rapid response characteristics of deadbeat control, and the disturbance rejection capabilities of repetitive control. The proposed controller offers an advanced solution by reducing the coupling effects, mitigating disturbances, and providing deadbeat response without the need of a delay compensation.

The combination of these three controllers (PI, deadbeat, and repetitive) takes use of their respective capabilities to improve overall system performance. The PI controller's decoupling mechanism simplifies the control process by efficiently reducing the effects of cross-coupling, thus providing more stable control. The deadbeat controller contributes to the system's fast dynamic response, enabling it to swiftly counteract any unexpected changes in system parameters. Meanwhile, the repetitive controller addresses periodic disturbances, such as harmonics caused by renewable energy sources, resulting in a cleaner and more steady power output. By combining these functionalities, the proposed hybrid controller not only improves the E-STATCOM's ability to efficiently regulate active and reactive power but also enhances its flexibility to varying grid conditions and disturbances. The key advantages of the proposed hybrid controller are summarized below:

- Reduced effects of cross-coupling.
- Wider control bandwidth and faster dynamic response.
- Improved regulation of output current, output powers, and DC-link voltage.
- Lower harmonic distortions.

The remaining sections in this paper are organized as follows. Section II explains the theory behind the control of E-STATCOM. Section III introduces the repetitive controller and presents the formulation of the proposed hybrid controller. Section IV discusses the experimental findings obtained using a three-phase E-STATCOM. Finally, Section V presents the conclusion.

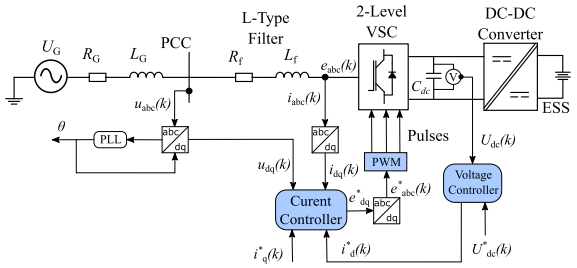

FIGURE 1. E-STATCOM control structure.

II. THEORY

Fig. 1 shows the E-STATCOM structure and its current-control scheme. The system's operation begins with the simultaneous monitoring of key parameters, including the VSC current, DC-link voltage, and grid voltage at the point of common coupling (PCC). A phase-locked loop (PLL) is employed to continuously monitor and synchronize with the grid frequency, enabling the extraction of the reference phase angle from the grid voltage. This phase angle serves as a fundamental parameter for performing Park-Clarke transformations, which are essential for voltage and current analysis. The transformed dq currents and voltages are fed to the controller. The DC-link voltage regulator maintains a constant DC-link voltage and produces the d-component current reference. The q-component current reference is produced by the AC voltage regulator or the reactive power controller. The DC-DC converter, on the other hand, is separately controlled to charge and discharge the ESS.

The dynamic voltage equation of a grid-connected STATCOM discretized over one switching interval of T_{sw} can be given as:

$$e_{\text{abc}}(k) = \frac{L_{\text{f}}}{T_{\text{sw}}}[i_{\text{abc}}(k+1) - i_{\text{abc}}(k)] + R_{\text{f}} i_{\text{abc}}(k) + u_{\text{abc}}(k) \tag{1}$$

where k denotes the discrete time step, L_{f} and R_{f} are the filter inductor and resistor, respectively, i_{abc} is the three-phase current, and u_{abc} is the three-phase grid voltage. In the discrete-time, the inductor current at $(k+1)_{\text{th}}$ step is equal to the reference current at k_{th} step; that is, $i^{*}_{\text{abc}}(k) = i_{\text{abc}}(k+1)$. Therefore, (1) can be written as:

$$e_{\text{abc}}(k) = \frac{L_{\text{f}}}{T_{\text{sw}}} i_{\text{err}}(k) + R_{\text{f}} i_{\text{abc}}(k) + u_{\text{abc}}(k) \tag{2}$$

where $i_{\text{err}}(k) = i^{*}_{\text{abc}}(k) - i_{\text{abc}}(k)$. Applying Clarke-Park's transformation, (2) can be written in the dq-frame as:

$$\begin{aligned} e_{\text{d}}(k) &= \frac{L_{\text{f}}}{T_{\text{sw}}} i_{\text{d,err}}(k) + R_{\text{f}} i_{\text{d}}(k) - \omega L_{\text{f}} i_{\text{q}}(k) + u_{\text{d}}(k) \\ e_{\text{q}}(k) &= \frac{L_{\text{f}}}{T_{\text{sw}}} i_{\text{q,err}}(k) + R_{\text{f}} i_{\text{q}}(k) + \omega L_{\text{f}} i_{\text{d}}(k) + u_{\text{q}}(k) \end{aligned} \tag{3}$$

where e_{d}, e_{q} and u_{d}, u_{q} are the E-STATCOM and the grid voltage, respectively, and i_{d}, i_{q} and $i_{\text{d,err}}$, $i_{\text{q,err}}$ are the E-STATCOM output currents and the error currents, respectively, in the dq-frame. The voltage equation in (3) distinctly reveals the cross-coupling terms, highlighting the interconnectedness of system variables.

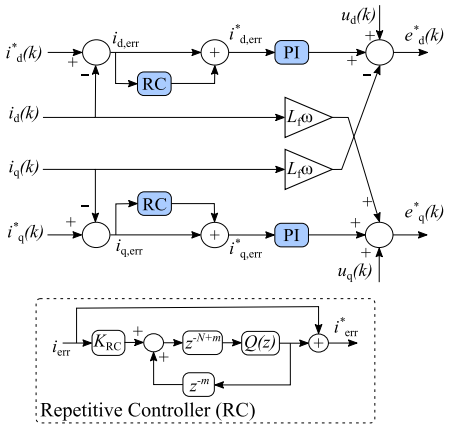

FIGURE 2. Conventional current controller schematic.

III. METHODS

A. CONVENTIONAL CURRENT CONTROLLER

Fig. 2 shows the conventional decoupled PI current controller integrated with an RC. The dotted rectangle depicts the plug-in RC scheme with phase lead compensation. This plug-in RC structure is a combination of the RC applied in [22] and [23]. The plug-in RC is then integrated with a traditional PI controller to implement the conventional controller. The PI control gains of the conventional controller are tuned on the basis of output filter parameters by applying the loop-shaping technique to have a cross-over frequency of 2 kHz.

The discrete transfer function of the plug-in RC can be derived as:

$$\text{G}_{\text{rc}}(z) = K_{\text{rc}} \frac{z^{-N+m}}{1 - z^{-N}} Q(z) \tag{4}$$

where K_{rc} is the controller gain, z^{-N} is the time delay unit, z^{m} is the time advance unit, and $Q(z)$ is a low pass filter. The stability and operation of the plug-in RC mainly relies on these parameters [23]. The modified internal model in (4) integrates the error on a periodic basis while the RC gain (K_{rc}) determines how fast the error converges [24].

$Q(z)$ has a zero-phase shift at low frequencies that improve the stability of the system by reducing the peak gains of the RC [25]. $Q(z)$ has the form of a typical first-order filter given as:

$$Q(z) = \alpha_1 z + \alpha_0 + \alpha_1 z^{-1} \tag{5}$$

where $\alpha_0 + 2\alpha_1 = 1$ and $\alpha_0, \alpha_1 > 0$. The time advance unit z^{m} performs the phase-lead compensation to improve the error convergence rate and tracking accuracy, especially at high frequencies. By employing a time delay unit z^{-N}, the system introduces a one-repeating period delay to the control action, which is expressed as:

$$N = \frac{f_{\text{s}}}{f} \tag{6}$$

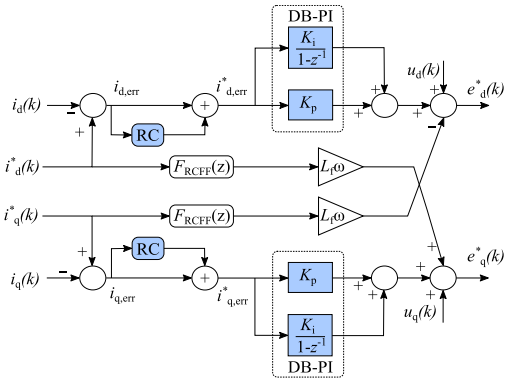

FIGURE 3. Proposed hybrid current controller schematic.

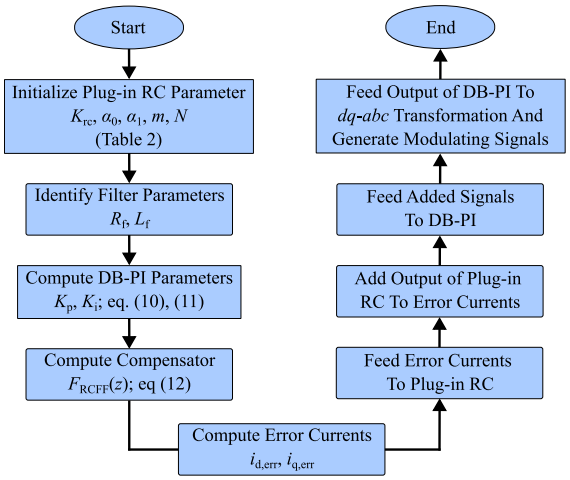

FIGURE 4. Step-by-step process modeling of the proposed controller.

where f_s is the sampling frequency and f is the reference frequency (grid frequency).

B. PROPOSED HYBRID CURRENT CONTROLLER

The proposed current controller is designed in the similar way as the conventional controller. The same plug-in RC is applied to the proposed controller. However, the PI control gains, in this case, are directly calculated using the output filter parameters to achieve the deadbeat characteristics.

According to [26], the continuous-time output of a PI controller to regulate the error signal $e(t)$ is written as:

$$u(t) = K_p e(t) + K_i \int_0^t e(\tau) d\tau \tag{7}$$

where K_p and K_i are the proportional and integral control gains, respectively. The PI controller transfer function can be derived by applying the Laplace tranform to (7) as:

$$C(s) = K_p + \frac{K_i}{s} \tag{8}$$

Applying backward-difference method, the controller in (8) can be discretized as:

$$C(z) = \frac{(K_p + K_i)z - K_p}{z - 1} \tag{9}$$

Based on the findings of [27], the PI control gains necessary to achieve the deadbeat characteristic can be derived as:

$$K_p = R_f \left(\frac{1}{1 - \exp\left(-\frac{R_f}{L_f} T_{sw}\right)} - 1 \right) \tag{10}$$

$$K_i = \frac{R_f}{T_{sw}} \tag{11}$$

where R_f and L_f are the output filter resistance and inductance, respectively, and T_{sw} is the switching period. Hence, by applying (10) and (11) to (9), the controller becomes a PI-based deadbeat (DB-PI) controller.

Fig. 3 shows the proposed current-control scheme. The proposed current controller integrates the plug-in RC with the DB-PI controller, employing the reference current feed-forward (RCFF) decoupling technique. In the proposed controller, the DB-PI ensures a fast dynamic response and the plug-in RC rejects the undesired periodic disturbances. Furthermore, the RCFF decoupling technique minimizes the effects of cross-coupling, reducing the transients in the active and reactive power, as well as the DC-link voltage [28]. The RCFF decoupling is realized by processing the reference current through the compensator $F_{RCFF}(z)$, instead of the previously implemented filter inductor current. The compensator $F_{RCFF}(z)$, defined in [29], is a second-order discrete filter with low-pass characteristics given by:

$$F_{RCFF}(z) = \frac{\omega_{ci} T_s (5 + 4z^{-1} - z^{-2})}{10 - \omega_{ci} T_s + (4\omega_{ci} T_s - 12)z^{-1} + (5\omega_{ci} T_s + 2)z^{-2}} \tag{12}$$

where ω_{ci} signifies the frequency at which the control loop gain crosses over to unity, that can be approximated as 5 % of the sampling frequency f_s, and T_s is the sampling period.

Fig. 4 shows the step-by-step modeling process of the proposed controller. The algorithm starts by initializing the Plug-in RC parameters. In the next step, the output filter parameters are identified, and the DB-PI control gains are computed along with the decoupling compensator. Next, the error currents are computed in the dq-frame and fed to the plug-in RCs. The plug-in RCs process the error signals, and the outputs are added back to their respective error signals. Then, the added signals are fed to their respective DB-PI controllers. Finally, the controller output signals are transformed back to three-phase signals and fed to the pulse-width modulator (PWM), which generates the switching signals.

C. BASIS OF COMPARISON

Three key performance metrics - namely controller bandwidth, dynamic performance, and harmonic rejection capability - are utilized to evaluate the effectiveness of the proposed controller. Firstly, the controller bandwidth provides valuable insights into the controller's responsiveness

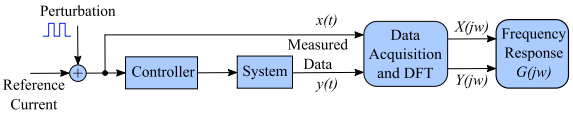

FIGURE 5. Frequency response measurement setup.

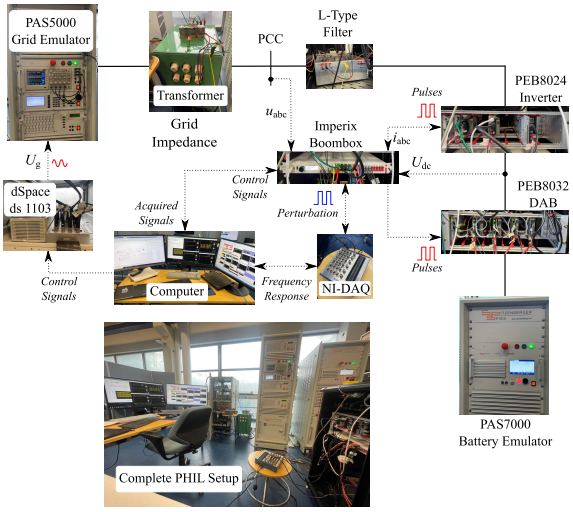

FIGURE 6. Experimental PHIL setup of the E-STATCOM.

to dynamic system variations. Secondly, the dynamic performance analysis evaluates the controller's efficacy in regulating current, voltage, and power. Lastly, the harmonic rejection capability assesses the controller's proficiency in mitigating the undesired disturbances, which provides insights into the controller's effectiveness at maintaining system stability.

In this study, the estimation of the controller bandwidth for the STATCOM application is conducted by measuring the control-to-output frequency response [30]. Fig. 5 depicts an illustration of the technique to obtain the frequency response by applying an external perturbation. This method involves superimposing an excitation current on the controller reference current. The resulting output current response $y(t)$ and the applied injection $x(t)$ are measured simultaneously. Subsequently, discrete Fourier transformed (DFT) is applied to the acquired signals to obtain the control-to-output frequency response $G(jw)$ as:

$$G(jw) = \frac{Y(jw)}{X(jw)} \tag{13}$$

where $X(jw)$) and $Y(jw)$ indicate the Fourier transform of $x(t)$ and $y(t)$, respectively. This method makes it possible to obtain the controller bandwidth rapidly and accurately in a practical application.

IV. EXPERIMENTAL RESULTS

A. SYSTEM SETUP

Fig. 6 illustrates the experimental setup for power hardware-in-the-loop (PHIL) implemented in this study. The grid emulator is independently controlled through dSPACE to generate a phase voltage of 120 V RMS. Similarly, the ESS is simulated using a battery emulator, which is controlled separately through the Imperix control platform. The functionality of the ESS is achieved through the utilization of a custom-built bi-directional dual active bridge (DAB) converter. The three-phase Imperix inverter serves as a STATCOM where the control is implemented by the Imperix Boombox.

TABLE 1. System parameters.

Grid	
Grid frequency, f	60 Hz
Grid voltage, U_g	120 V
Grid inductor, L_g	380 μH
Grid resistor, R_g	0.4 Ω
E-STATCOM	
Switching frequency, f_{sw}	18 kHz
Sampling frequency, f_s	18 kHz
Filter inductor, L_f	2.5 mH
Filter resistor, R_f	22 mΩ
DC-link capacitor, C_{dc}	780 μF
DC-link voltage, U_{dc}	400 V

TABLE 2. Plug-in RC parameters.

K_{rc}	N	m	$Q(z)$
0.6	300	2	$0.25z + 0.5 + 0.25z^{-1}$

The E-STATCOM was operated by applying a 4 A q-component current reference to provide reactive power compensation to the grid. Whereas, the d-component current reference was generated by the DC-link voltage controller. In addition, the bi-directional DAB was independently controlled to provide active power support to the grid. Table 1 provides detailed information on the system values and the operating point.

Three experiments were performed. The first experiment compared the effective controller bandwidth measured using both conventional and the proposed controller. The second experiment compared the dynamic response of the two controllers, during a step change in the reference current. Lastly, the third experiment compared the response of both controllers in the presence of a periodic disturbance. For a fair comparison, the parameters of the plug-in RC presented in Table 2 was implemented in both controllers. The values for the plug-in RC were selected based on the findings of [23].

B. EXPERIMENT 1: CONTROLLER BANDWIDTH COMPARISON

In the first experiment, the efficiency of the proposed controller was evaluated using the controller bandwidth. To obtain the controller bandwidth, an excitation signal was injected and the output response was collected using a measurement unit (NiDAQ-6363.) Fig. 7 shows the q-component control-to-output frequency response measured

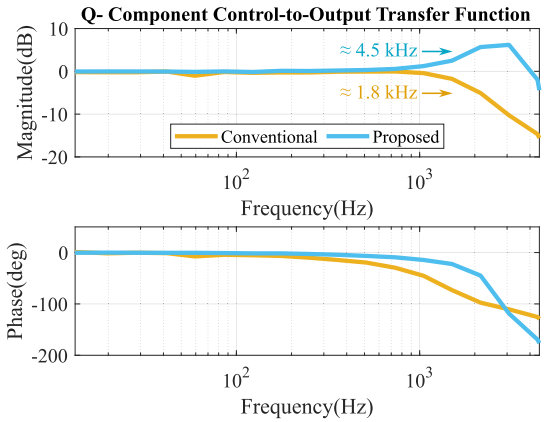

FIGURE 7. Comparison of controller bandwidth.

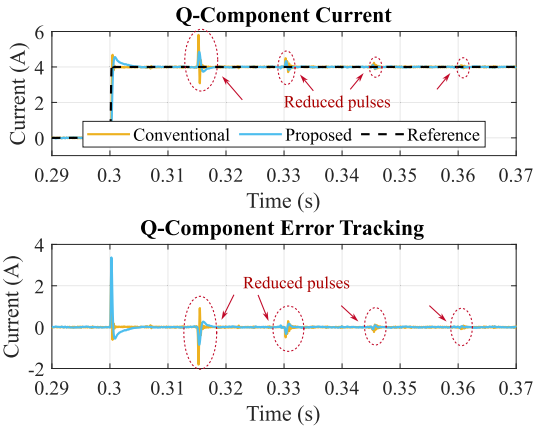

FIGURE 8. Q-component current and its error signal during step response.

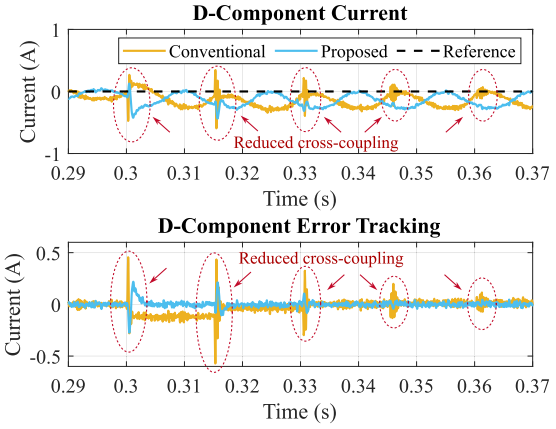

FIGURE 9. D-component current and its error signal during step response.

using both the conventional and the proposed controller. The controller bandwidth shows how fast the controller can react to changes in the system parameters. Moreover, the bandwidth defines the frequency spectrum over which the controller can maintain effective regulation. As the figure shows, the bandwidth of the proposed controller is much higher than the conventional controller. The findings suggest that the bandwidth of the conventional controller is approximately 1.8 kHz. Whereas, the proposed controller provides approximately 4.5 kHz bandwidth, that is, an increase of 150 % in comparison to the conventional controller. As a result, the proposed controller provides an improved response time and a much wider operating range. This indicates that the proposed controller is much more robust to the variations in the system dynamics.

One of the main benefits of having a larger bandwidth can be seen in the error tracking shown in experiment 2. However, one should be careful in the control design as the proposed controller tends to have higher resonance (seen in Fig. 7) which is generally not good because the controller amplifies the frequencies around this area. This means that when designing the proposed controller, one must be careful not to create too large resonance. One of the design criteria here is that one must stay within some predefined limits regarding the resonance.

C. EXPERIMENT 2: DYNAMIC RESPONSE COMPARISON

In this experiment, a 4 A step change is applied to the q-component current reference at $t = 0.3$ s and the dynamic response of conventional and the proposed controller is investigated. Fig. 8 shows the q component current and its error tracking during the applied step change. As the figure shows, the plug-in RC introduces pulses (visible at $t = 0.315$ s, $t = 0.33$ s, $t = 0.345$ s, and $t = 0.36$ s) in the q-component current. This is mainly caused by the control algorithm of the plug-in RC, which involves a delay and a feedback loop that tries to match the fundamental frequency of the system. Evidently, the proposed controller significantly reduces these undesired pulses and provides much better regulation compared to the conventional controller.

Fig. 9 shows the d-component current and its error tracking during a step change in the q-component current. As the figure shows, the proposed controller reduces the periodic pulses in both the d-component current and its error signal. This signifies that the proposed controller significatnly reduces the effects of cross-coupling in comparison to the conventional controller. In addition, the proposed controller provides superior error tracking, especially during the step change (from $t = 0.3$ s to $t = 0.315$ s).

Fig. 10 shows the E-STATCOM active and reactive powers during the applied step change in the q-component current. As the figure shows, the undesired pulses in the dq currents are reflected in the active and reactive powers. The proposed controller reduces the undesired effects of the cross-coupling and the periodic pulses from the active and reactive powers, respectively, in comparison to the conventional controller.

Fig. 11 shows the impact of the current controller on the dynamics of the DC-link voltage. A stable DC-link voltage is crucial for the system's robustness and effective power regulation to ensure smooth grid integration. As the figure shows, the proposed controller significantly mitigates

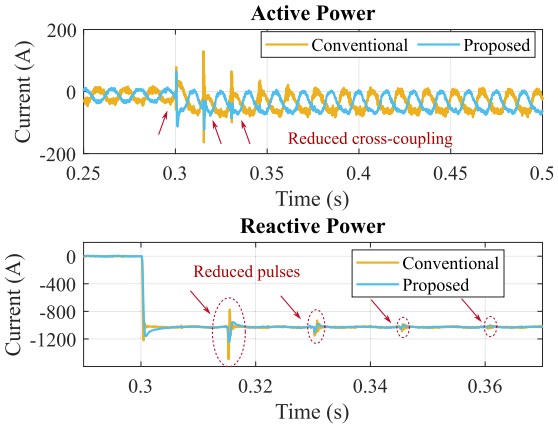

FIGURE 10. Active and reative power during step response.

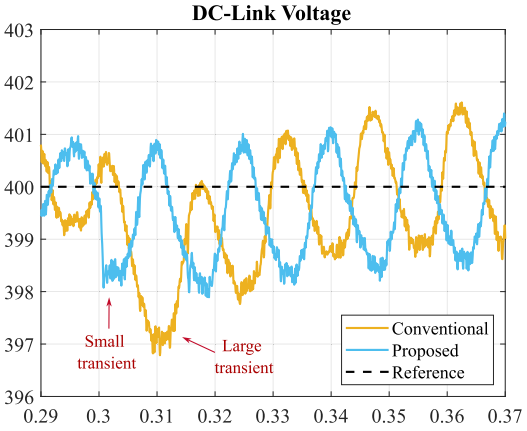

FIGURE 11. DC-link voltage during step response.

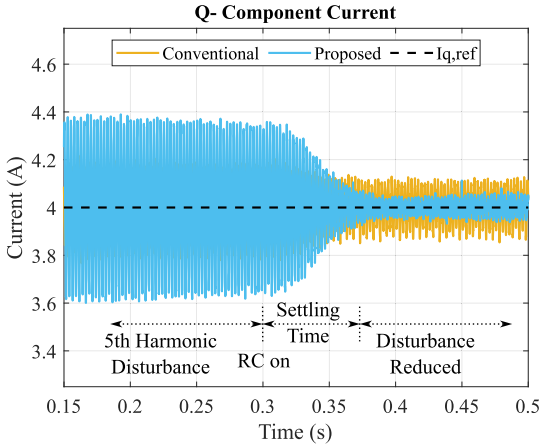

FIGURE 12. Dynamic response in the presence of periodic disturbance.

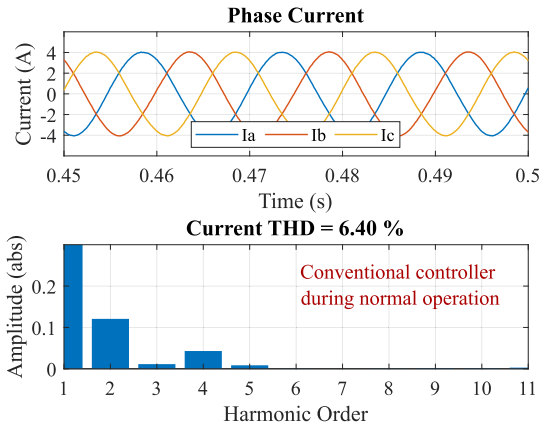

FIGURE 13. Current THD during normal operation using conventional controller.

transients in the DC-link voltage. Furthermore, the proposed controller allows the DC-link voltage to stabilize more quickly compared to the conventional controller, especially during abrupt changes in the current reference.

D. EXPERIMENT 3: RESPONSE TO PERIODIC DISTURBANCE

In this experiment, the responses of the conventional and proposed controllers were compared in the presence of a periodic disturbance, such as the fifth harmonic. First, the E-STATCOM is operated normally to provide the reactive power support. Then, a negative sequence fifth harmonic is added to the grid voltage. The presence of fifth harmonics in the grid voltage introduces harmonic components into the output current. These harmonics causes distortions to the current waveform, leading to increased THD that can degrade the power quality and affect the performance of the E-STATCOM.

Fig. 12 shows the q-component current response of both controllers when the plug-in RC is activated at $t = 0.3$ s. As the figure shows, the q-component current has a high harmonic content before the plug-in RC is activated due to the presence of the fifth harmonic. As the plug-in RC is activated, the RC feedback loop compares the actual output current with the desired current over several fundamental cycles and generates the compensation signal to counteract the periodic disturbance. Evidently, the proposed controller significantly attenuates the disturbance, exhibiting its superiority over the conventional controller.

Furthermore, a THD analysis was conducted on the output current obtained using both conventional and the proposed controller. This investigation focused on examining the current waveforms and their associated harmonic spectra up to the eleventh harmonic under two distinct operational conditions: normal operating condition and during a harmonic disturbance.

Fig. 13 and 14 show the output current waveforms and their corresponding harmonic spectra under normal operating conditions, employing the conventional and proposed controllers, respectively. Similarly, Fig. 15 and 16 present the output current waveforms and harmonic spectra during the harmonic disturbance using each controller. As the figures demonstrate, the amplitudes of each harmonic order are reduced using the proposed controller compared to the conventional controller. This reduction in the harmonic amplitudes underscores the

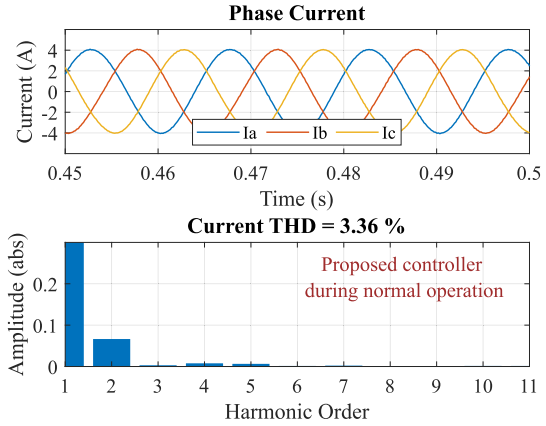

FIGURE 14. Current THD during normal operation using proposed controller.

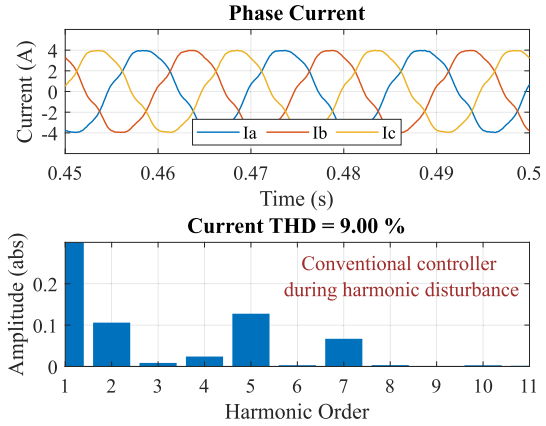

FIGURE 15. Current THD during harmonic disturbance using conventional controller.

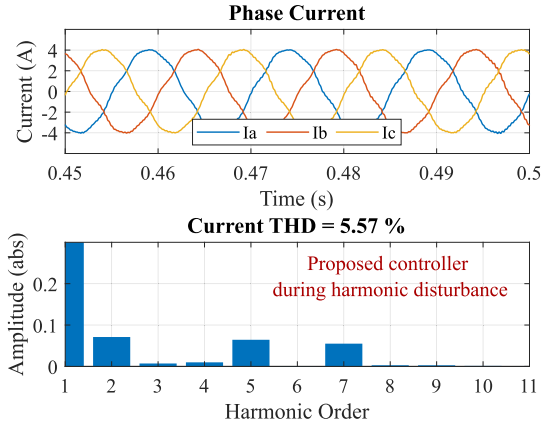

FIGURE 16. Current THD during harmonic disturbance using proposed controller.

remarkable efficacy of the proposed controller in attenuating current distortions, notably observed in both normal and disturbance-induced operational scenarios.

A summary of the THD values of the E-STATCOM output current using both conventional and the proposed controller are shown in Table 3. The data indicates that the conventional controller provides higher THD values with or without the presence of the fifth harmonic. Conversely, the proposed controller is able to keep the THD values below 6 % in either cases. Moreover, the proposed controller reduces the output current THD by 38 % to 47 % when compared to the conventional controller.

TABLE 3. Output current THD values with and without periodic disturbance (fifth harmonic).

5^{th} Harmonic	Conventional [22], [23]	Proposed	THD Reduction
No	6.40 %	3.36 %	47.5 %
Yes	9.00 %	5.57 %	38.11 %

V. CONCLUSION

Energy-storage equipped STATCOM (E-STATCOM) is an important device applied in various electrical power systems to regulate active and reactive power. The device combines the benefits of traditional STATCOM technology with energy-storage capabilities, thus offering enhanced voltage control and power quality management.

This paper has presented a novel hybrid current controller to be applied with E-STATCOM devices. The proposed current controller combines the strengths of the PI, deadbeat, and the repetitive controllers. By integrating the decoupling mechanism from the PI current controller, rapid response attributes of the deadbeat current controller, and the harmonic rejection capability of the repetitive controller, the proposed controller provides a much more robust and efficient solution for STATCOM applications. The proposed controller minimizes the cross-coupling effects and also delivers deadbeat response, a wide control bandwidth, and an efficient disturbance rejection.

The experimental findings validate the efficacy of the proposed current controller, establishing its superiority over the conventional controller. The higher bandwidth of the proposed controller indicates its ability to provide faster and more efficient response to the variations in the system parameters. The dynamic response study, together with the THD analysis, reveals that the proposed controller outperforms the conventional controller in regulating the current and mitigating the unwanted harmonic disturbances.

Building on these promising results, future work will investigate the proposed contoller's performance in comparison to other hybrid controllers, especially during frequency variations and unbalanced grid voltage. Additionally, future research will focus on further optimizing the proposed controller for any inverter-based application. This includes exploring adaptive control strategies based on real-time parameter identification.

REFERENCES

[1] R. K. Varma, E. Siavashi, S. Mohan, and J. McMichael-Dennis, "Grid support benefits of solar PV systems as STATCOM (PV-STATCOM) through converter control: Grid integration challenges of solar PV power systems," *IEEE Electrific. Mag.*, vol. 9, no. 2, pp. 50–61, Jun. 2021.

[2] T. Ahmed, A. Waqar, E. A. Al-Ammar, W. Ko, Y. Kim, M. Aamir, and H. U. R. Habib, "Energy management of a battery storage and D-STATCOM integrated power system using the fractional order sliding mode control," *CSEE J. Power Energy Syst.*, vol. 7, no. 5, pp. 996–1010, Sep. 2021.

[3] N. R. Merritt, C. Chakraborty, and P. Bajpai, "An E-STATCOM based solution for smoothing photovoltaic and wind power fluctuations in a microgrid under unbalanced conditions," *IEEE Trans. Power Syst.*, vol. 37, no. 2, pp. 1482–1494, Mar. 2022.

[4] M. Parvez, M. F. M. Elias, N. A. Rahim, and N. Osman, "Current control techniques for three-phase grid interconnection of renewable power generation systems: A review," *Sol. Energy*, vol. 135, pp. 29–42, Oct. 2016.

[5] M. I. Mosaad, H. S. M. Ramadan, M. Aljohani, M. F. El-Naggar, and S. S. M. Ghoneim, "Near-optimal PI controllers of STATCOM for efficient hybrid renewable power system," *IEEE Access*, vol. 9, pp. 34119–34130, 2021.

[6] G. Elhassan, S. A. Zulkifli, S. Z. Iliya, H. Bevrani, M. Kabir, R. Jackson, M. H. Khan, and M. Ahmed, "Deadbeat current control in grid-connected inverters: A comprehensive discussion," *IEEE Access*, vol. 10, pp. 3990–4014, 2022.

[7] P. Mattavelli, L. Tubiana, and M. Zigliotto, "Torque-ripple reduction in PM synchronous motor drives using repetitive current control," *IEEE Trans. Power Electron.*, vol. 20, no. 6, pp. 1423–1431, Nov. 2005.

[8] M. Pichan, M. Seyyedhosseini, and H. Hafezi, "A new DeadBeat-based direct power control of shunt active power filter with digital implementation delay compensation," *IEEE Access*, vol. 10, pp. 72866–72878, 2022.

[9] L. Ren, F. Wang, Y. Shi, and L. Gao, "Coupling effect analysis and design principle of repetitive control based hybrid controller for SVG with enhanced harmonic current mitigation," *IEEE J. Emerg. Sel. Topics Power Electron.*, vol. 10, no. 5, pp. 5659–5669, Oct. 2022.

[10] Y. Yang, Y. Yang, L. He, M. Fan, Y. Xiao, R. Chen, M. Xie, X. Zhang, L. Zhang, and J. Rodriguez, "A novel cascaded repetitive controller of an *LC*-filtered H6 voltage-source inverter," *IEEE J. Emerg. Sel. Topics Power Electron.*, vol. 11, no. 1, pp. 556–566, Feb. 2023.

[11] B. A. Francis and W. M. Wonham, "The internal model principle for linear multivariable regulators," *Appl. Math. Optim.*, vol. 2, no. 2, pp. 170–194, Jun. 1975.

[12] M. Jamil, A. Waris, S. O. Gilani, B. A. Khawaja, M. N. Khan, and A. Raza, "Design of robust higher-order repetitive controller using phase lead compensator," *IEEE Access*, vol. 8, pp. 30603–30614, 2020.

[13] B. Han, S.-W. Jo, M. Kim, N. A. Dung, and J.-S. Lai, "Improved odd-harmonic repetitive control scheme for cuk-derived inverter," *IEEE Trans. Power Electron.*, vol. 37, no. 2, pp. 1496–1508, Feb. 2022.

[14] S. Kolluri, N. B. Y. Gorla, and S. K. Panda, "Capacitor voltage ripple suppression in a modular multilevel converter using frequency-adaptive spatial repetitive-based circulating current controller," *IEEE Trans. Power Electron.*, vol. 35, no. 9, pp. 9839–9849, Sep. 2020.

[15] C. Tan, Q. Chen, L. Zhang, and K. Zhou, "Frequency-adaptive repetitive control for three-phase four-leg V2G inverters," *IEEE Trans. Transport. Electrific.*, vol. 7, no. 4, pp. 2095–2103, Dec. 2021.

[16] T. Wang, J. Zheng, Q. Chen, Y. Liu, and W. Song, "Mitigation of subsynchronous control interaction in DFIG-based wind farm using repetitive-PI," *IEEE Access*, vol. 11, pp. 60807–60816, 2023.

[17] M. Tian, B. Wang, Y. Yu, Q. Dong, and D. Xu, "Discrete-time repetitive control-based ADRC for current loop disturbances suppression of PMSM drives," *IEEE Trans. Ind. Informat.*, vol. 18, no. 5, pp. 3138–3149, May 2022.

[18] B. Chen, Z. Huang, P. Sun, and G. Wei, "Harmonic suppression for PMSM applied to MSTMP based on virtual even-order fractional repetitive controller," *IEEE Trans. Ind. Informat.*, vol. 20, no. 4, pp. 6289–6299, Apr. 2024.

[19] J. S. Costa, A. Lunardi, L. F. Normandia Lourenço, and A. J. Sguarezi Filho, "Robust predictive repetitive current control for a grid-connected inverter under parametric uncertainty," *IEEE J. Emerg. Sel. Topics Power Electron.*, vol. 11, no. 5, pp. 4693–4703, Jul. 2023.

[20] A. Lunardi, E. Conde, J. Assis, L. Meegahapola, D. A. Fernandes, and A. J. Sguarezi Filho, "Repetitive predictive control for current control of grid-connected inverter under distorted voltage conditions," *IEEE Access*, vol. 10, pp. 16931–16941, 2022.

[21] P. Liu, C. Wang, Y. Zhang, Y. Liang, Y. Cui, and J. Fang, "Frequency adaptive repetitive control of new energy grid-connected inverter based on improved IIR," *IEEE Trans. Power Electron.*, vol. 38, no. 8, pp. 9539–9551, Aug. 2023.

[22] Q. Zhao, Y. Ye, G. Xu, and M. Zhu, "Improved repetitive control scheme for grid-connected inverter with frequency adaptation," *IET Power Electron.*, vol. 9, no. 5, pp. 883–890, Apr. 2016.

[23] B. Zhang, D. Wang, K. Zhou, and Y. Wang, "Linear phase lead compensation repetitive control of a CVCF PWM inverter," *IEEE Trans. Ind. Electron.*, vol. 55, no. 4, pp. 1595–1602, Apr. 2008.

[24] L. He, K. Zhang, J. Xiong, and S. Fan, "A repetitive control scheme for harmonic suppression of circulating current in modular multilevel converters," *IEEE Trans. Power Electron.*, vol. 30, no. 1, pp. 471–481, Jan. 2015.

[25] Q. Zhao, H. Zhang, Y. Gao, S. Chen, and Y. Wang, "Novel fractional-order repetitive controller based on thiran IIR filter for grid-connected inverters," *IEEE Access*, vol. 10, pp. 82015–82024, 2022.

[26] K. Heong Ang, G. Chong, and Y. Li, "PID control system analysis, design, and technology," *IEEE Trans. Control Syst. Technol.*, vol. 13, no. 4, pp. 559–576, Jul. 2005.

[27] S. Kuroda, K. Natori, and Y. Sato, "PI current control method for realizing deadbeat characteristics," in *Proc. Int. Power Electron. Conf. (IPEC-Himeji ECCE Asia)*, May 2022, pp. 57–62.

[28] H. Basnet, T. Roinila, H. Hafezi, R. Sallinen, and M. Tran, "Decoupled control to improve DC-link dynamics of energy-storage-equipped STATCOM," in *Proc. Int. Conf. Smart Energy Syst. Technol. (SEST)*, Sep. 2022, pp. 1–6.

[29] S. Zhou, J. Liu, L. Zhou, and Y. Zhang, "DQ current control of voltage source converters with a decoupling method based on preprocessed reference current feed-forward," *IEEE Trans. Power Electron.*, vol. 32, no. 11, pp. 8904–8921, Nov. 2017.

[30] H. Basnet, M. Berg, M. Tran, and T. Roinila, "Rapid online identification of non-linear current-controller bandwidth in STATCOM application," in *Proc. IEEE Energy Convers. Congr. Expo. (ECCE)*, Oct. 2023, pp. 1012–1017.

HIKMAT BASNET (Graduate Student Member, IEEE) received the M.Sc. (Tech.) degree in electrical engineering from Tampere University, Tampere, Finland, in 2021, where he is currently pursuing the Ph.D. degree with the Faculty of Information Technology and Communication Sciences.

His main research interests include modeling and control of grid-connected power-electronics systems.

TOMI ROINILA (Member, IEEE) received the M.Sc. (Tech.) and Dr.Tech. degrees in automation and control engineering from Tampere University of Technology, Tampere, Finland, in 2006 and 2010, respectively.

He is currently an Associate Professor with Tampere University, Tampere. His main research interests include modeling and control of grid-connected power-electronics systems, analysis of energy-storage systems, modeling of multiconverter systems, and condition monitoring and online identification of power electronic converters.